JOURNAL OF SOLID STATE CHEMISTRY 108, 402–409 (1994)

Synthesis, Structure, and Properties of the Layered Perovskite $La_3Ni_2O_{7-\delta}$

Z. Zhang, M. Greenblatt,[1] and J. B. Goodenough

Department of Chemistry, Rutgers, The State University of New Jersey, Piscataway, New Jersey 08855; Center for Materials Science ETC 9.102, The University of Texas at Austin, Austin, Texas 78712

Received April 12, 1993; in revised form June 17, 1993; accepted June 18, 1993

Single-phase samples of $La_3Ni_2O_{7-\delta}$ with $\delta = 0$, 0.08, and 0.65 were prepared and characterized by powder X-ray diffraction, TGA, electrical resistivity, and magnetic susceptibility. The crystal symmetry of the as-prepared ($\delta = 0.08$) and oxygenated ($\delta = 0.00$) samples is orthorhombic (space group *Fmmm*). Oxidation of the as-prepared $La_3Ni_2O_{6.92}$ sample to $La_3Ni_2O_{7.00}$ shows little change in the unit-cell parameters. Reduction of $La_3Ni_2O_{6.92}$ to $La_3Ni_2O_{6.35}$ results in a structural phase transition from orthorhombic to tetragonal symmetry, a dramatic decrease in the *c* cell parameter, and significant increase in the *a* and *b* cell parameters. These data are consistent with loss of oxygen from the apical octahedral sites connecting two perovskite layers in $La_3Ni_2O_{7-\delta}$. The electrical transport properties change with decreasing oxygen content from metallic for $La_3Ni_2O_{7.00}$ to semiconducting for $La_3Ni_2O_{6.92}$ and $La_3Ni_2O_{6.35}$. The fully reduced sample, $La_3Ni_2O_{6.35}$, shows a linear dependence of ln ρ versus $T^{-1/4}$ in the temperature range 90–140 K, suggesting a variable-range hopping mechanism. A nearly temperature-independent magnetic susceptibility is observed in the temperature range 100–300 K for the $\delta = 0$ and 0.08 samples. The relatively high values and the temperature dependence of the magnetic susceptibility indicate a Stoner enhanced Pauli paramagnetism for $\delta = 0$ and evidence for a weak ferromagnetism in the $\delta = 0.65$ sample. The electrical and magnetic properties of $La_3Ni_2O_{7-\delta}$ are discussed in terms of the mixed-valent character of nickel and vacancy-induced localization effects.

INTRODUCTION

A rich variety of oxides classified as Ruddlesden–Popper (1) (RP) phases are described as intergrowth structures having the general formula $(AO)(ABO_3)_n$, where *A* is usually a rare-earth, alkaline-earth, or alkali ion and *B* can be a 3*d* or 4*d* transition-metal ion. Common to this class of structures is the stacking of *n* ABO_3 perovskite layers between rock-salt *AO* layers along the crystallographic *c*-axis (Fig. 1). The transport properties of various members within a given series are governed primarily by the identity and valence of the transition-metal ion, the width *n* of the ABO_3 perovskite slabs, the *B*–O–*B* bond angle, and the oxygen content. For example, $LaNiO_3$ ($n = \infty$) is metallic, whereas $GdNiO_3$ is an antiferromagnetic semiconductor as a result of a decrease in the Ni–O–Ni bond angle with decreasing size of the lanthanide ion. La_2NiO_4, in which the corner-sharing NiO_6 octahedral units in the *ab* plane are sandwiched between the LaO rock-salt layers, is semiconducting below 500 K. The electrical conductivities of the intermediate members increase with *n*.

The recently discovered cuprate high-temperature superconducting oxides are closely related to the RP phases with ordered oxygen vacancies in the perovskite layers. In most of the cuprate superconductors, the transition temperature T_c increases with the number of perovskite layers up to $n = 4$. The superconductivity of the cuprates appears in a transition region between the insulating and normal-metal states (2, 3). The mixed-valent character of $La_{n+1}Ni_nO_{3n+1}$ ($n = 2$, 3 etc.) is similar to that of the cuprate superconductors. Although both $LaSrNiO_4$ and La_2CuO_4 have the same type of crystal structure and both low-spin Ni^{3+} ($t_{2g}^6e_g^1$) and Cu^{2+} ($t_{2g}^6e_g^3$) have one unpaired electron in an e_g orbital, the distribution of the single electron of Ni^{3+} among orbitals of $d_{x^2-y^2}$ and d_{z^2} symmetry differs from that of the single hole on the Cu^{2+} ion. The discovery of diamagnetism in $La_2NiO_{4+\delta}$ and $La_{2-x}M_xNiO_4$ (M = Sr, Ca) (4) compounds at low temperature has further stimulated extensive studies on the structure and properties of the nickelates. However, the difficulties associated with the synthesis of monophasic specimens of $(LnO)(LnNiO_3)_n$ for $n > 1$ have limited detailed studies on both their structure and physical properties (5, 6).

The objectives of the present investigation were (a) the optimization of the synthetic conditions leading to the formation of monophasic $La_3Ni_2O_{7-\delta}$, (b) the examination of the structural stability of this phase in controlled oxygen atmosphere, and (c) the systematic examination

[1] To whom correspondence should be addressed.

0022-4596/94 $6.00

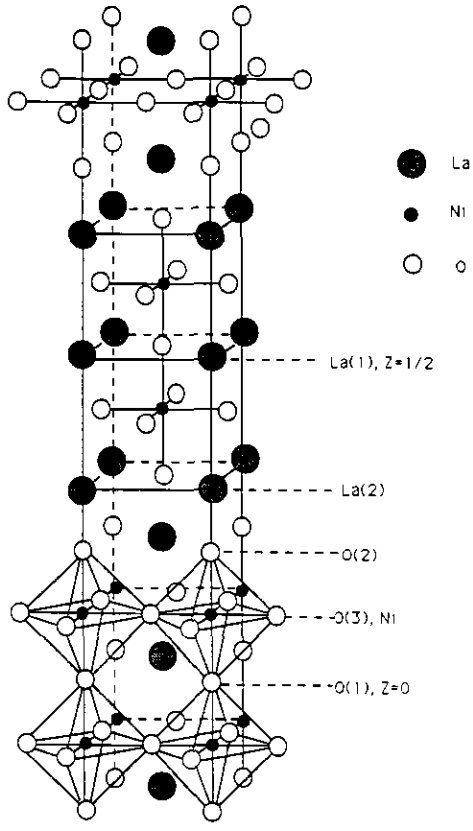

FIG. 1. The structure of $La_3Ni_2O_{7-\delta}$.

of the influence of the oxygen content on the transport properties of the $La_3Ni_2O_{7-\delta}$ compound.

EXPERIMENTAL

Single-phase $La_3Ni_2O_{7-\delta}$ was prepared by the following procedure: Stoichiometric amounts of NiO and precalcined La_2O_3 were dissolved in nitric acid (about 3 *M*) solution. A 25% aqueous solution of tetramethylammonium hydroxide was slowly added to this solution until a light-green precipitate formed. The solution containing the precipitate was gently heated to dryness on a hot plate. The resulting light-green powder was heated at 350°C in air to decompose the organic precursor. The dark-gray product was ground and pressed into pellets and heated in air at 1150–1200°C for 4–5 days in a high-density alumina crucible. Several intermittent grindings followed by repelletization were necessary to obtain single-phase $La_3Ni_2O_{7-\delta}$. The high-pressure oxygen annealing was carried out at 500°C under ~70 atm of oxygen for 24 hr in a Leco high-pressure apparatus. Hydrogen reduction was carried out at 450°C in flowing 11% H_2 in N_2 or Ar (The purity of all the balance gases is 99.99%). Microstructural and compositional analysis was obtained with an Amray 1400 Scanning Electron Microscope (SEM) equipped with an energy-dispersal X-ray (EDX) analysis facility.

Powder X-ray diffraction (PXD) data collected with a SCINTAG PAD V diffractometer and Ni-filtered Cu$K\alpha$ radiation were used in the least-squares refinement of the unit-cell parameters. Mica and Mo were used as internal standards. Electrical resistivity of pressed pellets was measured in a standard four-probe configuration with a closed-cycle cryostat (APD Cryogenics, DE202) in the temperature range 20–300 K. A SQUID magnetometer (MPMS, Quantum design) was used to measure the magnetic susceptibility of samples in the temperature range 2–340 K in an applied magnetic field of 1000 G. The oxygen contents were determined with iodometric titration and thermogravimetric analysis (TGA) in a reducing atmosphere (11% H_2 in Ar) with a DuPont 951 thermogravimetric analyzer. In the TGA study, the heating rate was 3°C/min and the gas flow rate was about 35 cm^3/min.

RESULTS AND DISCUSSION

Synthesis

The conventional solid-state reaction between La_2O_3 and NiO in the mole ratio La : Ni = 1.5 : 1 in the temperature range 900–1400°C resulted in the formation of a mixture of $La_3Ni_2O_{7-\delta}$ with $La_2NiO_{4-\delta}$, $La_4Ni_3O_{10-\delta}$, and the starting materials. Similar attempts by Petrov *et al.* (5) and Seppanen (6) to prepare $La_3Ni_2O_{7-\delta}$ in this temperature range in air were also unsuccessful. Although there are reports regarding the structure and properties of $La_3Ni_2O_{7-\delta}$, these studies were made on impure samples (7–9). The critical conditions for the synthesis of pure $La_3Ni_2O_{7-\delta}$ are determined by several factors: the heating temperature and time, the oxygen partial pressure, the homogeneity of the starting materials, and the particle size. We were successful in preparing single-phase samples of $La_3Ni_2O_{7-\delta}$ reproducibly by the codecomposition of organic precusors. The advantage of this route over conventional ceramic methods is the homogeneous mixing of the starting materials and the small particle size of the reactants. The PXD pattern revealed that the product is monophasic. As a further check of the purity of the sample product, we have carried out detailed microstructural and compositional analysis by EDX on grains selected from random portions of different batches of samples. Polycrystalline La_2NiO_4 was used as a standard to minimize the matrix effect. The La : Ni ratio obtained from the EDX is 1.5 : 1 (within ±5%) across and within the grains, which indicates the compositional homogeneity of the samples.

The oxygen content of the as-prepared sample was determined by iodometric titration and TGA to correspond to $La_3Ni_2O_{6.92}$. Heating the as-prepared sample at high-

TABLE 1
The Lattice Parameters and Oxygen Content of $La_3Ni_2O_{7-\delta}$ Samples

Compound[a]	Space group	a (Å)	b (Å)	c (Å)	Annealing
$La_3Ni_2O_{7.00}$	*Fmmm*	5.396(1)	5.449(1)	20.516(4)	O_2
$La_3Ni_2O_{6.92}$	*Fmmm*	5.3961(6)	5.4498(5)	20.522(2)	Air
$La_3Ni_2O_{6.35}$	*Fmmm*	5.484(2)	5.479(2)	20.064(6)	H_2/Ar
	I4/mmm	3.8757(6)	3.8757(6)	20.062(6)	H_2/Ar

[a] The experimental error of δ is ±0.02.

pressure oxygen (~70 atm) and 500°C for 24 hr yielded $La_3Ni_2O_{7.00}$ as determined by TGA and iodometric titration. Sintering $La_3Ni_2O_{6.92}$ in 11% H_2/Ar flow at ~450°C afforded the fully reduced sample with a stoichiometry of $La_3Ni_2O_{6.35}$ again ascertained by TGA.

Structural Properties

The unit-cell parameters as a function of oxygen content of $La_3Ni_2O_{7-\delta}$ are summarized in Table 1. The cell parameters of the as-prepared $La_3Ni_2O_{6.92}$ sample obtained in this study are in good agreement with those reported in the literature (7, 8, 10, 11). For $La_3Ni_2O_{6.92}$ and $La_3Ni_2O_{7.00}$, the change of the lattice parameters is within the experimental error. Upon annealing the as-prepared $La_3Ni_2O_{6.92}$ in an H_2 atmosphere, a tetragonal phase (space group *I4/mmm*) $La_3Ni_2O_{6.35}$ is obtained with larger ***a*** and ***b*** parameters (indexed as a pseudo-orthorhombic cell, Table 1) and a dramatically smaller ***c*** parameter than that of the orthorhombic $La_3Ni_2O_{6.92}$. The large decrease of ~0.46 Å in the ***c*** unit-cell parameter of the reduced phase, $La_3Ni_2O_{6.35}$, relative to the as-prepared sample is attributed to loss of apical oxygens. Figure 1 shows that there are two types of apical oxygens in this structure: O(1) links two NiO_2 layers, while O(2) is associated with the LaO layers. The amount of oxygen lost in the reduction reaction, 0.65 mole/(formula unit) from $La_3Ni_2O_{7.00}$ to $La_3Ni_2O_{6.35}$, is consistent with a loss of 65% of the oxygen atoms from the O(1) site. The orthorhombic-to-tetragonal phase transition that occurs upon reduction of $La_3Ni_2O_{6.92}$ to $La_3Ni_2O_{6.35}$ is clearly shown by the PXD pattern in Fig. 2. A similar phase transformation is observed upon the reduction of the n = 3, $La_4Ni_3O_{10}$ phase (12).

The atomic positions of La, Ni, and O were generated for $La_3Ni_2O_{6.92}$ (with a tetragonal-to-orthorhombic transformation matrix) and $La_3Ni_2O_{6.35}$ from the known positional parameters of $Sr_3V_2O_7$ (13). Table 2 shows the atomic positions in both phases. All the atomic positions except O(3) are the same in both *Fmmm* and *I4/mmm* space groups. The Lazy-Pulverix program was used to generate the theoretical diffraction patterns of $La_3Ni_2O_{6.92}$ and $La_3Ni_2O_{6.35}$ based on these atomic positions. The observed PXD patterns for $La_3Ni_2O_{6.35}$ and $La_3Ni_2O_{6.92}$ are shown in Fig. 2. The PXD data are summarized in Tables 3 and 4. The agreement between the theoretical and experimental intensities for both phases is in general satisfactory considering that the atomic positions are not refined and that any preferred orientation effects are neglected. Varying the occupancy of the O(1) site by using the Lazy-Pulverix program to calculate the intensities of PXD does not seem to affect significantly any of the reflections. In this structure, that includes heavy ions like La, it would be unexpected to refine the occupancy factors of the oxygens from PXD data.

Lacorre (12) suggested that in $La_4Ni_3O_{10}$, the n = 3 RP analogue of $La_3Ni_2O_{7-\delta}$, the reduction to $La_4Ni_3O_8$ leads to a shifting of the apical oxygens linking the La–O layers

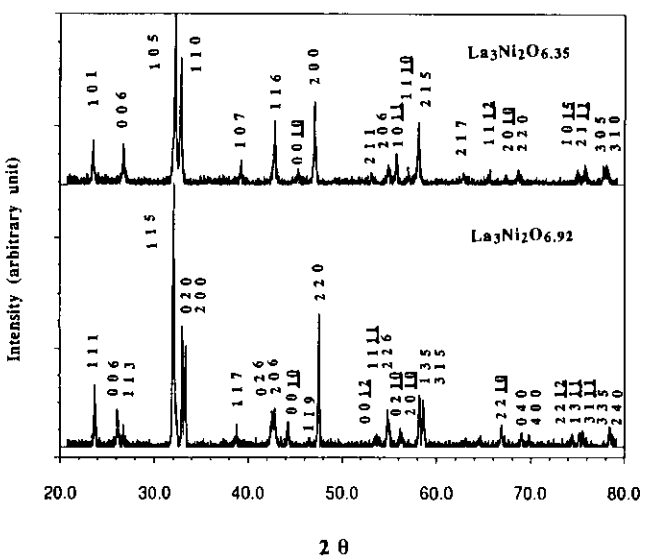

FIG. 2. X-ray powder patterns of $La_3Ni_2O_{6.92}$ (space group *Fmmm*) and $La_3Ni_2O_{6.35}$ (space group *I4/mmm*).

TABLE 2
Positional Coordinates of La, Ni, and O in $La_3Ni_2O_{6.92}$ (Space Group *Fmmm*) and $La_3Ni_2O_{6.35}$ (Space Group *I4/mmm*)

Atoms	x	y	z	Site (O)	Site (T)
La(1)	0	0	0.5	4*b*	2*b*
La(2)	0	0	0.3148(3)	8*i*	4*e*
Ni	0	0	0.0971(7)	8*i*	4*e*
O(1)	0	0	0	4*a*	2*a*
O(2)	0	0	0.190(2)	8*i*	4*e*
O(3)[T]	0	0.5	0.096(2)	—	8*g*
O(3)[O]	−0.25	0.25	0.096(2)	16*j*	—

Note. T, the tetragonal $La_3Ni_2O_{6.35}$ (space group *I4/mmm*). O, The orthorhombic $La_3Ni_2O_{6.92}$ (space group *Fmmm*).

TABLE 3
Powder X-Ray Diffraction Data of $La_3Ni_2O_{6.92}$ (Space Group *Fmmm*)

h	*k*	*l*	d_{obs} (Å)	d_{calc} (Å)	Δd (Å)	I_{obs}	I_{calc}[a]
1	1	1	3.768	3.769	0.001	19	15
0	0	6	3.421	3.420	−0.001	12	10
1	1	3	3.342	3.345	0.003	5	5
1	1	5	2.803	2.802	−0.001	100	100
0	2	0	2.725	2.725	0	47	30
2	0	0	2.699	2.698	−0.001	39	29
1	1	7	2.329	2.329	0	7	4
0	2	6	2.130	2.131	0.001	12	13
2	0	6	2.118	2.118	0	13	13
0	0	10	2.053	2.052	−0.001	8	13
1	1	9	1.959	1.960	0.001	2	2
2	2	0	1.917	1.917	0	47	34
1	3	1	—	1.716	—	—	2
0	0	12	1.711	1.710	−0.001	3	2
3	1	1	1.700	1.702	0.002	2	2
1	1	11	1.677	1.678	0.001	11	8
2	2	6	1.673	1.672	−0.001	5	6
0	2	10	1.639	1.639	0	5	8
2	0	10	1.634	1.633	−0.001	3	8
1	3	5	1.588	1.588	0	18	19
3	1	5	1.577	1.577	0	17	18
0	2	12	—	1.445	—	—	2
2	0	12	1.444	1.445	0.001	3	2
2	2	10	1.401	1.401	0	7	14
0	4	0	1.362	1.362	0	4	5
4	0	0	1.349	1.349	0	4	5
1	1	15	—	1.289	—	—	3
2	2	12	1.276	1.276	0	3	3
1	3	11	1.265	1.265	0	4	4
3	1	11	1.260	1.260	0	5	4
3	3	5	1.221	1.220	−0.001	6	8
2	4	0	1.217	1.216	−0.001	4	5
4	2	0	—	1.209	—	—	5

[a] All reflections with relative theoretical intensity greater than 2% are listed.

(O(2) in our paper) and results in a *T'*-type structure, in which the Ni^{n+} ions are in a square-planar coordination. A calculation considering a *T'* model for $La_3Ni_2O_{6.35}$ resulted in a significantly poorer agreement of the experimental and calculated intensities of the PXD. Therefore a transition to a *T'*-type structure in $La_3Ni_2O_{6.35}$ is ruled out.

Thermogravimetric Analysis and Post Annealing

Thermogravimetric analysis (TGA) for all three samples (δ = 0, 0.08, and 0.65) and iodometric titration for the δ = 0 and 0.08 samples were used to determine the oxygen content and the phase transition. A common feature of the reduction curves of $La_3Ni_2O_{6.92}$ and $La_3Ni_2O_{7.00}$ was the two-step behavior illustrated in Fig. 3. The first plateau in the weight-loss curve is associated

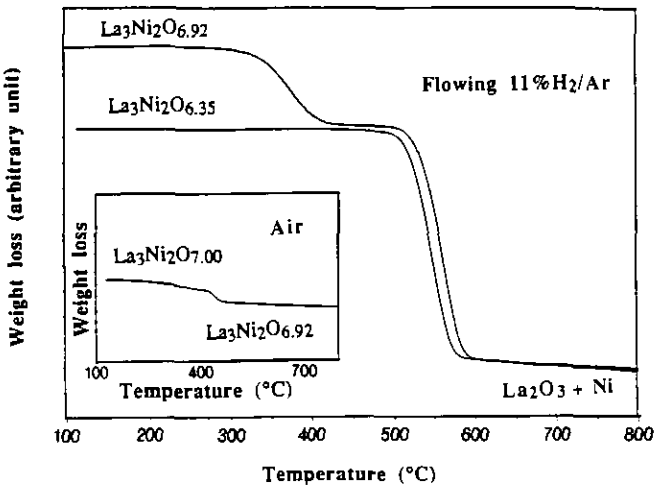

FIG. 3. TGA weight loss curves for $La_3Ni_2O_{6.92}$ and $La_3Ni_2O_{6.35}$ in H_2/Ar and for $La_3Ni_2O_{7.00}$ in air (inset).

with the stabilization of an intermediate phase corresponding to the composition of $La_3Ni_2O_{6.35}$ in the temperature range 400–520°C. This small window of the temperature provides the annealing conditions for obtaining samples with controlled oxygen contents (i.e., δ = 0,

TABLE 4
Powder X-Ray Diffraction Data of $La_3Ni_2O_{6.35}$ (Space Group *I4/mmm*)

h	*k*	*l*	d_{obs} (Å)	d_{calc} (Å)	Δd (Å)	I_{obs}	I_{calc}[a]
1	0	1	3.805	3.806	0.001	24	16
0	0	6	3.342	3.344	0.002	19	10
1	0	5	2.789	2.788	−0.001	100	100
1	1	0	2.739	2.741	0.002	66	62
1	0	7	2.304	2.304	0	10	3
1	1	6	2.699	2.698	−0.001	28	26
0	0	10	2.008	2.006	−0.002	3	11
2	0	0	1.938	1.938	0	44	33
2	1	1	1.728	1.727	−0.001	6	4
2	0	6	1.676	1.677	0.001	8	6
0	0	12	—	1.672	—	—	2
1	0	11	1.650	1.650	0	14	7
1	1	10	1.617	1.619	0.002	5	13
2	1	5	1.591	1.591	0	33	34
2	1	7	—	1.483	—	—	2
1	1	12	1.428	1.427	−0.001	2	3
2	0	10	1.394	1.394	0	3	11
2	2	0	1.369	1.370	0.001	2	8
2	2	6	—	1.268	—	—	2
2	0	12	—	1.266	—	—	3
1	0	15	—	1.264	—	—	2
2	1	11	1.256	1.256	0	3	6
3	1	0	1.226	1.226	0	5	8

[a] All reflections with relative theoretical intensity greater than 2% are listed.

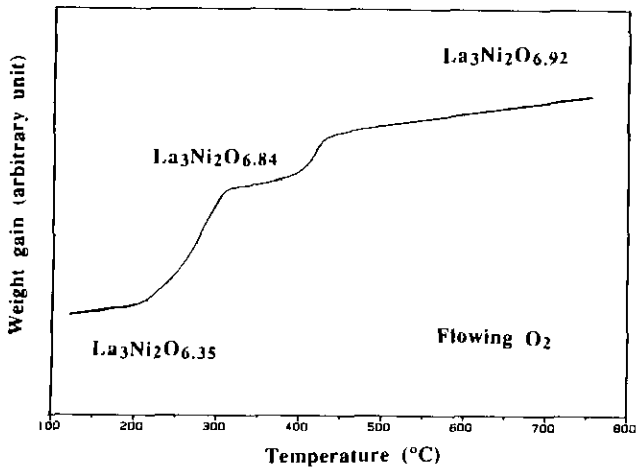

FIG. 4. TGA weight gain curve for $La_3Ni_2O_{6.35}$ in flowing O_2.

0.08, 0.65). The second weight loss with onset at 520°C corresponds to the decomposition of the $La_3Ni_2O_{6.35}$ phase. Alternatively, the fully reduced phase $La_3Ni_2O_{6.35}$ shows a single weight-loss feature with onset at 520°C, which corresponds to the decomposition of the sample (Fig. 3).

The extent of reduction with the same hydrogen content in the same temperature range was found to depend on the balance gas. In an 11% H_2/Ar atmosphere, the sample is reduced to $\delta = 0.65$, while in an 11% H_2/N_2 stream it is reduced to $\delta = 0.16$. Higher temperatures result in the decomposition of the sample in both cases. The lower reduction ability in the presence of N_2 gas may be due to adsorption of N_2 on the sample surface or to some other mechanisms, which prevent the reduction.

Sintering any of the oxygen-deficient samples ($\delta = 0.08$ or 0.65) at high pressure of O_2 (~70 atm/500°C) results in the fully oxygenated $La_3Ni_2O_{7.00}$. When the oxygenated sample $La_3Ni_2O_{7.00}$ is sintered in air (~425°C), $La_3Ni_2O_{6.92}$ forms (Fig. 3, inset). Similarly, when tetragonal $La_3Ni_2O_{6.35}$ is sintered in flowing O_2 gas at 1 atm (~425°C), orthorhombic $La_3Ni_2O_{6.92}$ is obtained (Fig. 4). Thus the phase transition/oxygen stoichiometry is reversible:

$$La_3Ni_2O_{6.35} \underset{H_2/Ar/450°C}{\overset{\text{Flow } O_2/425°C}{\rightleftharpoons}} La_3Ni_2O_{6.92} \underset{\text{air}/425°C}{\overset{\text{high pressure } O_2/500°C}{\rightleftharpoons}} La_3Ni_2O_{7.00}. \quad (1)$$

$$La_3Ni_2O_{6.84} \underset{H_2/N_2/450°C}{\overset{\text{Flow } O_2/425°C}{\rightleftharpoons}} La_3Ni_2O_{6.92}$$

Obviously, $La_3Ni_2O_{6.92}$ is the thermodynamically stable phase in air. The final products of the TGA, analyzed by X-ray powder diffraction, were La_2O_3 and Ni. The oxygen contents of all the samples were estimated from the total weight loss and are listed in Table 1. Iodometric titration was also carried out on the same sample batch of $La_3Ni_2O_{7.00}$ and $La_3Ni_2O_{6.92}$ as that used for the TGA data as well as on a different sample batch. The difference in oxygen content found by the two methods (TGA and iodometric titration) is within the experimental error.

Electrical Transport Properties and Band Structure

The room-temperature (RT) resistivity (ρ) of $La_3Ni_2O_{7-\delta}$ has been previously reported (8, 9, 11) to range from 0.01 to 1 ohm-cm, varying with the oxygen uncertainty. The magnitude of the room-temperature resistivity of all the polycrystalline samples in this study and their temperature dependence are summarized in Table 5.

The room-temperature resistivity increases dramatically with decreasing oxygen content in $La_3Ni_2O_{7-\delta}$, demonstrating the influence of oxygen content on the electronic transport properties. The nearly stoichiometric and fully oxidized sample of $La_3Ni_2O_{7.00}$ exhibits metallic behavior while both oxygen-deficient samples are semiconducting (Figs. 5 and 6). In the Ni-based Ruddlesden–Popper phases, the $3d$ electrons of the Ni ions, which determine the transport property (14), could be either localized or itinerant (15, 16), depending on the

TABLE 5
The Electrical Properties of $La_3Ni_2O_{7-\delta}$

Compounds	Annealing atmosphere	RT resistivity (ohm-cm)	Temperature dependence	E_a (eV) (250 K < T < 290)
$La_3Ni_2O_{7.00}$	O_2	0.01–0.02	Metallic	—
$La_3Ni_2O_{6.92}$	Air	0.2–0.4	Semiconductor	0.01
$La_3Ni_2O_{6.35}$	H_2/Ar	200–300	Semiconductor	0.15

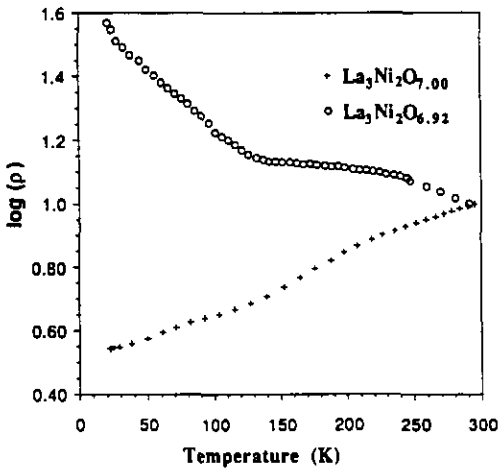

FIG. 5. Temperature dependence of resistivity for $La_3Ni_2O_{7.00}$ and $La_3Ni_2O_{6.92}$.

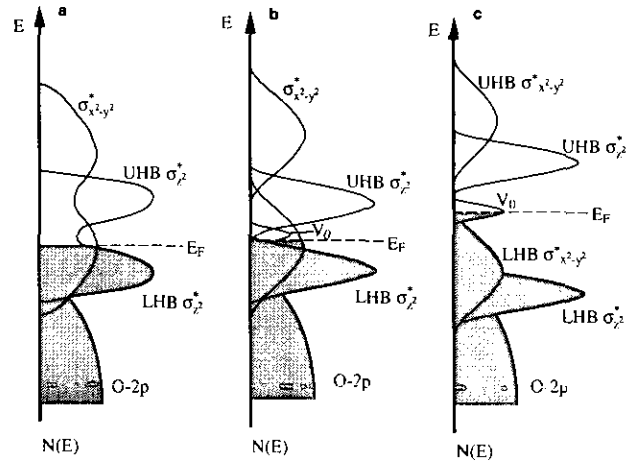

FIG. 7. Schematic energy density of states near the Fermi energy E_F for $La_3Ni_2O_{7-\delta}$ (V_0 = oxygen vacancy): (a) $La_3Ni_2O_{7.00}$. (b) $La_3Ni_2O_{6.92}$. (c) $La_3Ni_2O_{6.35}$.

Ni valence/oxygen stoichiometry and the geometry of the structure (i.e., the electronic band structure). The schematic band diagram for $La_3Ni_2O_{7.00}$ shown in Fig. 7a reflects the mixed Ni^{3+}/Ni^{2+} formal valence in which strong hybridization of the σ-bonding Ni–3*d* and O–2*p* orbitals creates narrow antibonding σ^* bands. The shorter Ni–O(3) bonds (ca. 1.92 Å) in the basal plane relative to the *c*-axis Ni–O(1) and Ni–O(2) bond lengths (ca. 1.97 Å) suggest that the $\sigma^*_{z^2}$ band ($z \| c$) is narrower and its orbitals lie somewhat lower in energy than the $\sigma^*_{x^2-y^2}$ orbitals. Should the $\sigma^*_{z^2}$ band be half filled and exhibit a correlation splitting into an upper and lower Hubbard band (UHB and LHB), we should nevertheless expect the observed metallic conductivity due to a $\sigma^*_{x^2-y^2}$ band only one-quarter filled.

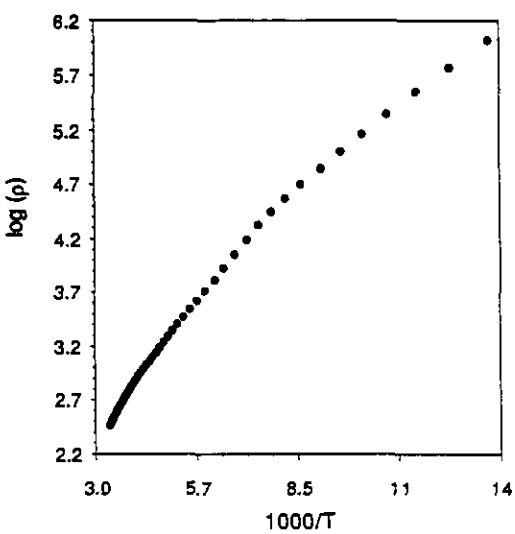

FIG. 6. Inverse temperature dependence of log (ρ) for $La_3Ni_2O_{6.35}$.

The appearance of a distinguishable thermodynamic phase $La_3Ni_2O_{6.92}$ suggests a change in the character of the $\sigma^*_{z^2}$ and/or $\sigma^*_{x^2-y^2}$ orbitals. The introduction of oxygen vacancies perturbs strongly the periodic Ni-site potential; the vacancies introduce two-electron traps for the $\sigma^*_{z^2}$ electrons and introduce Anderson localization of states at the edges of the $\sigma^*_{x^2-y^2}$ band and, if split by strong correlations, in the middle of the correlation gap, as illustrated in Fig. 7b. Reduction introduces 0.08 electrons/atom into the σ^* bands, which is not enough to inhibit strong mixed-valent conduction in the narrow $\sigma^*_{x^2-y^2}$ band; but the presence of localized states near E_F can be expected to introduce a weak semiconductive temperature dependence of the conductivity at lower temperatures.

Further reduction to the semiconductor phase $La_3Ni_2O_{6.35}$ stabilizes a phase with localized 3*d* electrons (Fig. 7c). What is curious is that this phase is not stabilized for a single valent Ni^{2+} configuration but for the formal valences $La_3Ni^{2+}_{1.7}Ni^{1+}_{0.3}O_{6.35}$. Access to the mixed Ni^{2+}/Ni^{1+} redox couple is made possible by the oxygen vacancies; they trap a single electron ca. 1 eV below the $\sigma^*_{z^2}$ UHB. In the $La_3Ni_2O_{6.35}$ phase, about half of the oxygen vacancy traps are occupied by an electron, and a variable-range hopping between vacancies (17) can be anticipated in the conduction mechanism. A linear dependence of ln ρ vs $T^{-1/4}$ is observed below 140 K (Fig. 8), which is consistent with a variable-range hopping mechanism. A similar complex evolution of resistivity with temperature has been observed in the intergrowth structure $Sr_4V_3O_{10}$ (18).

The quasi-two-dimensional structure of $La_3Ni_2O_{7-\delta}$ can be expected to give a highly anisotropic conductivity. More detailed discussion of the transport properties must await measurements on single-crystal samples.

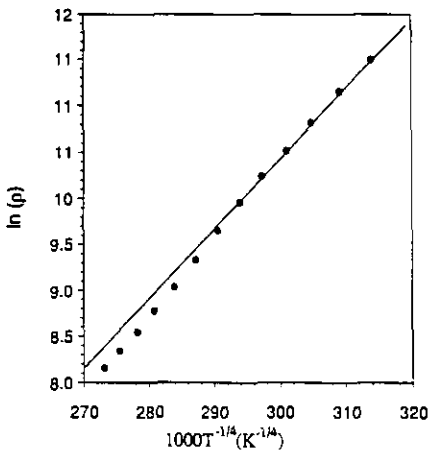

FIG. 8. $1000T^{(-1/4)}$ dependence of ln (ρ) for $La_3Ni_2O_{6.35}$.

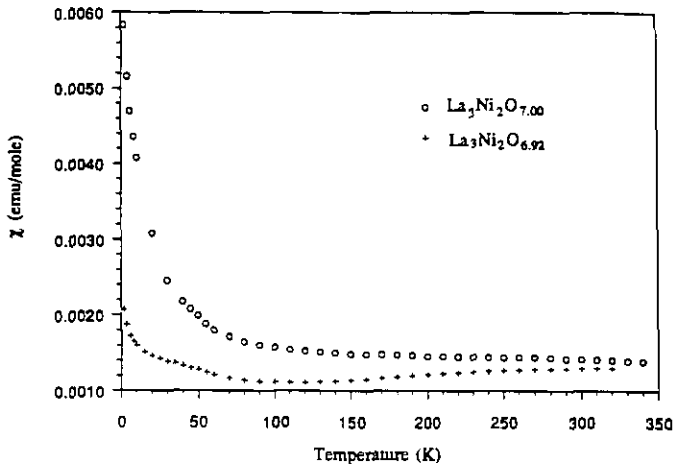

FIG. 9. Temperature dependence of susceptibility for $La_3Ni_2O_{7.00}$ and $La_3Ni_2O_{6.92}$.

Magnetic Susceptibility

The magnetic susceptibility χ, measured as a function of the temperature for the samples of $La_3Ni_2O_{6.92}$ and $La_3Ni_2O_{7.00}$, is shown in Fig. 9. The room-temperature susceptibility values of $La_3Ni_2O_{7.00}$ and $La_3Ni_2O_{6.92}$ are the same within experimental error. The high values of the susceptibility from 100–300 K in Fig. 9 can be attributed to a Stoner enhancement due to ferromagnetic correlations among electrons in an $\sigma^*_{x^2-y^2}$ band about one-quarter filled (19). The susceptibility of $La_3Ni_2O_{7.00}$ remains nearly independent of the temperature in the temperature range 100–300 K, consistent with Pauli-paramagnetic behavior. The χ of $La_3Ni_2O_{6.92}$ decreases slightly with decreasing temperature in the same temperature range. This phenomenon of decreasing χ with decreasing temperature in the high-temperature region has also been observed in La_2NiO_4 (20) where it has been attributed to short-range antiferromagnetic order when the $\sigma^*_{x^2-y^2}$ bands are half filled. In $La_3Ni_2O_{6.92}$, the relative increase in the occupancy of the $\sigma^*_{x^2-y^2}$ bands may introduce antiferromagnetic interactions (19) and a short-range antiferromagnetic order consistent with narrower σ^* bands. Below 100 K, paramagnetic behavior caused by electrons localized at oxygen vacancies dominates the susceptibility of both compounds.

In Fig. 10, the variation of χ with temperature of the fully reduced phase $La_3Ni_2O_{6.35}$ below 350 K shows a complex behavior. The susceptibility is quite high and increases with decreasing temperature. These features are characteristic of a ferromagnetic material. The field dependence of susceptibility at 100 K on $La_3Ni_2O_{6.35}$ shows a strong deviation from linear behavior and a saturation above 4000 G, which is also evidence of weak ferromagnetism. The ferromagnetic property of the $La_3Ni_2O_{6.35}$ sample may be due to trace amounts of Ni that cannot be detected by PXD. Based on the room-temperature values of the susceptibility, ~0.7% (by weight) of Ni would be present in the sample. On the other hand, localization of the σ^* electrons in $La_3Ni_2O_{6.35}$ itself must give a nickel atomic moment.

CONCLUSION

We have successfully synthesized single-phase $La_3Ni_2O_{6.92}$ by a precursor method. $La_3Ni_2O_{7.00}$ was prepared from the $La_3Ni_2O_{6.92}$ sample at high-pressure (~70 atm) oxygen. Phases with $\delta = 0.16$ and 0.65 were also prepared from $La_3Ni_2O_{6.92}$ in a reducing atmosphere. From the X-ray powder diffraction data, the symmetry of the as-prepared sample $La_3Ni_2O_{6.92}$, the oxygenated $La_3Ni_2O_{7-\delta}$, and the partially reduced $La_3Ni_2O_{6.84}$ is

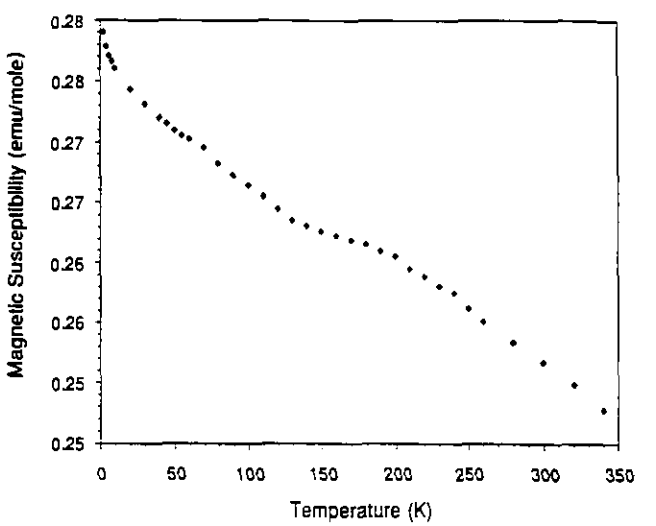

FIG. 10. Temperature dependence of susceptibility for $La_3Ni_2O_{6.35}$.

orthorhombic with space group *Fmmm*. The cell parameters ***a***, ***b***, and ***c*** vary only within the experimental error upon the oxidation of the as-prepared sample. Upon reduction of $La_3Ni_2O_{6.92}$ to $La_3Ni_2O_{6.35}$, a structural phase transition from orthorhombic-to-tetragonal symmetry occurs. The significant decrease of the ***c*** parameter of the reduced phase is due to the loss of *c*-axis oxygens, most probably the bridging apical oxygens connecting the Ni atoms of a double-perovskite layer. The oxidation/reduction reactions via oxygen gain/loss are completely reversible. $La_3Ni_2O_{7-\delta}$ with $\delta = 0$ is metallic near a metal insulator transition. The $\delta = 0.08$ phase exhibits semiconducting behavior caused by the induction of localized states of the oxygen vacancies. In the fully reduced phase, $La_3Ni_2O_{6.35}$, the loss of ~65% of the oxygens in the apical position connecting the NiO_6 octahedra leads to a trapping of d_{z^2} electrons at oxygen vacancies with energies in the band gap region. Both activated and variable-range hopping mechanisms of electron transport are observed in the $\delta = 0.65$ phase. The temperature-independent paramagnetic behavior of $La_3Ni_2O_7$ is consistent with its metallic behavior. However both this $\delta = 0$ and the $\delta = 0.08$ phase have a relatively high magnetic susceptibilities in the temperature range 300–100 K, indicating a strong Stoner or mass enhancement of narrow-band electrons. The paramagnetic Curie tail in the susceptibility at low temperature is attributed to defect-induced electron localizations.

ACKNOWLEDGMENTS

This research was supported by National Science Foundation Solid State Chemistry Grant DMR-90-19301. The authors thank Dr. K. V. Ramanujachary for helpful discussions.

REFERENCES

1. S. N. Ruddlesden and P. Popper, *Acta Crystallogr.* **11,** 54 (1958).
2. H. Takagi, T. Ido, S. Ishibashi, M. Uota, and S. Uchida, *Phys. Rev. B* **40,** 2254 (1989).
3. H. Takagi, S. Uchida, and Y. Tokura, *Phys. Rev. Lett.* **62,** 1197 (1989).
4. K. S. Nanjundaswamy, A. Lewicki, Z. Kakol, P. Gopalan, P. Metcalf, J. M. Honig, C. N. R. Rao, and J. Spalek, *Physica C* **166,** 361 (1990).
5. A. N. Petrov, V. A. Cherepanov, A. Yu. Zuyev, and V. M. Zhukovsky, *J. Solid State Chem.* **77,** 1 (1988).
6. M. Seppanen, *Scand. J. Metall.* **8,** 191 (1979).
7. C. Brisi, M. Vallino, and F. Abbattista, *J. Less-Common Metals* **79,** 215 (1981).
8. V. F. Savhenko, L. S. Ivashkevich, and I. Ya. Lyubkina, *Russ. J. Inorg. Chem. (Engl. Transl.)* **33,** 17 (1988).
9. F. Gervais, P. Odier, and Y. Nigara, *Solid State Commun.* **56,** 371 (1985).
10. J. Drennan, C. P. Tavares, and B. C. H. Steele, *Mater. Res. Bull.* **17,** 621 (1982).
11. R. A. Mohan Ram, L. Ganapathi, P. Ganguly, and C. N. R. Rao, *J. Solid State Chem.* **63,** 139 (1986).
12. Ph. Lacorre, *J. Solid State Chem.* **97,** 495 (1992).
13. N. Suzuki, T. Noritake, N. Yamamoto, and T. Hioki, *Mater. Res. Bull.* **26,** 1 (1991).
14. J. B. Goodenough and S. Ramasesha, *Mater. Res. Bull.* **17,** 383 (1982).
15. P. Ganguly and C. N. R. Rao, *Mater. Res. Bull.* **8,** 405 (1973).
16. J. B. Goodenough, *Mater. Res. Bull.* **8,** 423 (1973).
17. N. F. Mott and E. A. Davis, "Electronic Processes in Non-Crystalline Materials," 2nd ed. Oxford Univ. Press, Oxford, 1979.
18. N. Ohashi, Y. Teramoto, H. Ikawa, O. Fukunaga, and J. Tanaka, *J. Solid State Chem.* **97,** 434 (1992).
19. J. B. Goodenough, *Prog. Solid State Chem.* **5,** 145 (1971).
20. C. N. R. Rao, D. J. Buttrey, N. Otsuka, P. Ganguly, H. R. Harrison, C. J. Sandberg, and J. M. Honig, *J. Solid State Chem.* **51,** 266 (1984).